

Initial validation of a soil-based mass-balance approach for empirical monitoring of enhanced rock weathering rates

Tom Reershemius^{1*} and Mike E. Kelland^{2*}, Jacob S. Jordan³, Isabelle R. Davis^{1,4}, Rocco D'Ascanio¹, Borianna Kalderon-Asael¹, Dan Asael¹, T. Jesper Suhrhoff^{5,1}, Dimitar Z. Epihov², David J. Beerling², Christopher T. Reinhard⁶, Noah J. Planavsky^{1,5}

¹Department of Earth and Planetary Sciences, Yale University, New Haven, CT, USA

²Leverhulme Centre for Climate Change Mitigation, School of Biosciences, University of Sheffield, Sheffield, UK

³Porecast Research, Lawrence, KS, USA

⁴School of Ocean and Earth Science, University of Southampton Waterfront Campus, Southampton, UK

⁵Yale Center for Natural Carbon Capture, Yale University, New Haven, CT, USA

⁶School of Earth and Atmospheric Sciences, Georgia Institute of Technology, GA, USA

*corresponding and equal contribution authors: tom.reershemius@yale.edu, mekelland1@sheffield.ac.uk.

Preprint: <https://doi.org/10.48550/arXiv.2302.05004>

Keywords: Enhanced Rock Weathering; Carbon Dioxide Removal; Negative Emissions Technology; Monitoring, Reporting and Verification; Climate Change Mitigation

Synopsis: We describe and empirically validate a geochemical mass-balance approach for tracking rates of Enhanced Rock Weathering in soils, a necessary step in scaling up a promising Carbon Dioxide Removal strategy.

Abstract: Enhanced Rock Weathering (ERW) is a promising scalable and cost-effective Carbon Dioxide Removal (CDR) strategy with significant environmental and agronomic co-benefits. A major barrier to large-scale implementation of ERW is a robust Monitoring, Reporting, and Verification (MRV) framework. To successfully quantify the amount of carbon dioxide removed by ERW, MRV must be accurate, precise, and cost-effective. Here, we outline a mass-balance-based method where analysis of the chemical composition of soil samples is used to track *in-situ* silicate rock weathering. We show that signal-to-noise issues of *in-situ* soil analysis can be mitigated by using isotope-dilution mass spectrometry to reduce analytical error. We implement a proof-of-concept experiment demonstrating the method in controlled mesocosms. In our experiment, basalt rock feedstock is added to soil columns containing the cereal crop *Sorghum bicolor* at a rate equivalent to 50 t ha⁻¹. Using our approach, we calculate rock weathering corresponding to an average initial CDR value of 1.44 ± 0.27 tCO₂eq ha⁻¹ from our experiments after 235 days, within error of an independent estimate calculated using conventional elemental budgeting of reaction products. Our method provides a robust time-integrated estimate of initial CDR, to feed into models that track and validate large-scale carbon removal through ERW.

1 Introduction

Avoiding 2°C of global warming by 2100 will require dramatic carbon emissions reduction, meaning governments must implement policies with increasingly stringent year-on-year carbon mitigation targets (1, 2). Even the full implementation of all emissions mitigation policies, as of 2022, will result in a 12 gigatonne (10^9 tonne) CO₂-equivalent shortfall to climate goals as outlined by the Paris Agreement (3). In the absence of feasible pathways to sufficiently reduce carbon emissions, large-scale Carbon Dioxide Removal (CDR) will likely be essential for augmenting decarbonization efforts in the coming century (e.g., 4,5).

Enhanced Rock Weathering (ERW) is a promising CDR technique where naturally occurring mineral weathering reactions that consume atmospheric CO₂ are accelerated. This may be achieved by applying crushed silicate rocks with a high reactive surface area to agricultural and forest soils (e.g., 6-21). Potential advantages and co-benefits of ERW include a low technological barrier to implementation at scale (8, 13); long-term storage of carbon compared to organic reservoirs (>10,000 years) (22-28); and supply of key nutrients for crop growth (13, 29-37). Additionally, ERW feedstocks such as basalt may be used for the deacidification of soils, filling the role of agricultural lime (currently a net source of CO₂ to the atmosphere; 38-46). Several recent studies have improved our understanding of ERW: mechanistic modelling of weathering reactions in agricultural soils (e.g., 11, 14, 47, 48); modelling hydrological effects on weathering rates (e.g., 49); laboratory and mesocosm experiments tracking uptake of nutrients by plants, and feedstock dissolution rates (e.g., 31, 33, 46, 50-56); and field experiments implementing ERW at scale (e.g., 35, 57-60).

Despite these recent advances, ERW currently lacks a robust and widely accepted framework for Monitoring, Reporting, and Verification (MRV) of CDR rates. This represents a significant barrier to widespread implementation of ERW, in voluntary or compliance markets, or as a subsidized agronomic practice. There will be strong variability in the rates of rock weathering in agricultural settings with variable hydroclimatic conditions, highlighting the need for empirical constraints on weathering at this stage (e.g., 61). Approaches to MRV that are entirely model-based are yet to be fully validated for ERW. The current generation of reactive transport models for simulating ERW have proven useful for making testable predictions (e.g., 14, 19, 47, 48). However, it is not yet clear whether such models are capable of accurately predicting CDR at deployment scale. Therefore, any modelling approach to estimate CDR through ERW at scale must have at its center a robust empirical MRV framework from a diverse set of environments to impart confidence to key stakeholders. The MRV framework must successfully report site- and time-specific rates of feedstock weathering while being cost-effective and minimally invasive (e.g., 62, 63).

In order to quantify weathering rates and/or initial CDR rates from ERW experiments, previous mesocosm and field studies have used measurements of soil inorganic carbon (e.g., 33, 55, 57, 59); the concentration of dissolved ions in porewaters and effluent waters, including cations such as Ca²⁺ and Mg²⁺, as well as carbonate alkalinity (e.g., 31, 33, 50-54, 56, 58, 59, 64); and Sr, Li, Mg, and C isotopic analysis of waters, soils, and rocks (e.g., 33, 51, 52, 59, 64). These data provide a valuable insight into the rate of weathering of feedstocks and the fate of reaction products at different stages of transport from topsoil to the river-ocean system, and it is therefore important that such measurements be made for a representative range of ERW deployment scenarios.

However, basing a site-specific empirical MRV protocol on these metrics is challenging: significant carbonate precipitation in soils is unlikely to occur within the pH range of most agricultural soils that require amendments for deacidification (as well as being undesirable); and collecting porewater and effluent water for analysis of field-specific weathering rates is time- and labor-intensive, and at watershed scale is only feasible in limited settings, such as zero-order streams (e.g., 59). For these reasons, such measurements likely cannot be used in every ERW deployment, if the technology is to scale.

Recent work using measurements of soil exchangeable cations and electrical conductivity as proxies for weathering and alkalinity generation respectively have been welcome steps toward building an MRV toolkit that meets the criteria for providing an empirical base in a wide range of agricultural ERW deployments, by tying in to existing agronomic practices or introducing practices that can be easily scaled (60, 65). However, there can be large errors associated with tracking alkalinity fluxes through electrical conductivity (see ref. 65, 66), while calculating weathering rates purely from the size of the soil exchangeable fraction presents a minimum weathering estimate.

Here, we add to this toolkit by introducing and providing an initial proof of concept study of a soil-based mass balance approach for quantitatively tracking enhanced rock weathering in soils. This approach measures the difference in concentration of ERW feedstock within a soil *in-situ* before and after weathering, directly building from techniques widely used to gauge the extent and mode of weathering in natural systems (e.g., 67-79). We compare the concentrations of mineral-bound metal cations (Ca^{2+} , Mg^{2+} , Na^+) in the solid phase of soils before and after feedstock deployment. We do this by estimating changes in the total amount of these metal cations (CAT) in a specific soil sample relative to the concentration of an immobile tracer, in this case titanium (Ti). Hereafter we refer to this method as TiCAT. As a first step towards robust validation, we compare estimates of the extent of *in-situ* basalt feedstock dissolution from TiCAT to rates determined independently from detailed pool and flux tracking (>2000 measurements) in a mesocosm experiment (following a similar method to that in ref. 33). We then discuss the practical considerations for this approach to be scaled for industrial scale deployment of CDR through ERW, and the steps require to move from an empirical estimate of feedstock dissolution rates to robust error-bounded estimates of CDR.

2 Materials and Methods

2.1 Theoretical Basis

TiCAT is a mass balance approach for estimating the time-integrated amount of weathering of a rock feedstock – in this case basalt – within a soil sample. This method builds on approaches for estimating the extent of weathering in natural systems, where the concentrations of mobile major cations in an unweathered parent material are compared to those in an equivalent amount of weathered material. The concentration of an immobile trace element is used to establish this equivalence (e.g., 67-79; see also *Supporting Information Section 1.9*). In the TiCAT framework, the unweathered parent material (basalt feedstock) is mixed into the soil. This presents a challenge, as in a field setting the amount of basalt present in a soil sample taken after deployment will not

necessarily be proportional to the total amount of basalt deployed, given soil mixing may not be perfectly homogeneous, and some erosion may occur.

To calculate the amount of unweathered parent material initially present in a sample taken after weathering of some of this material has occurred, we first compare soil samples after basalt amendment and weathering with soil samples representative of a pre-amendment baseline, as well as samples of the initial basalt feedstock. This can most readily be visualized as simple two-component mixing between a soil (c_s) and a basalt (c_b) endmember (**Fig. 1a**). We use the difference in concentration of an immobile trace element, i (e.g., Ti, which is widely used for this purpose, see 70, 80), between a post-application sample (c_{end}) and the pre-application soil baseline, to calculate the amount of basalt that has been added to the original soil for the specific sample analyzed ($[Ti]_{end} - [Ti]_s = [Ti]_{add}$). The assumption of immobility is critical to this approach, so while other elements could be used instead of Ti, it must be demonstrated that this criterion is met (see *Supporting Information Section 1.9*).

Using the relative abundance of Ti and mobile major cations (CAT) in the original basalt feedstock, we can then calculate the corresponding amount of mobile major cations, $[CAT]_{add}$, from the basalt feedstock present in the soil + basalt mixture at the point of basalt application (**Fig. 1b**). For a generic cation, CAT:

$$[CAT]_{add} = [Ti]_{add} \times \frac{[CAT]_b - [CAT]_s}{[Ti]_b - [Ti]_s}, \quad (1)$$

Subtracting the amount of cation in the post-application sample, $[CAT]_{end}$, and adding the soil baseline, $[CAT]_s$, we can calculate the difference in the amount of the mobile cation, $\Delta[CAT]$, between the expected amount from addition of basalt, and the observed amount in the soil + basalt mixture after weathering (**Fig. 1c**):

$$\Delta[CAT] = [CAT]_{add} + [CAT]_s - [CAT]_{end} \quad . \quad (2)$$

$\Delta[CAT]$ therefore represents the amount of cation loss due to basalt dissolution (i.e., exported from the solid phase) between the point of basalt application and the post-application sampling date. We can also define basalt dissolution as a fraction, F_D , where:

$$F_D = \frac{\Delta[CAT]}{[CAT]_{add}} \quad . \quad (3)$$

The concentration of Ti and CAT in samples may be affected by basalt dissolution reducing the mass of the system. Therefore, a correction for mass loss is applied to F_D (see *Supporting Information Section 1.9*). Multiplying F_D for each cation by the application rate of basalt-hosted CAT gives a cation-specific estimate for weathering of the basalt feedstock at the application scale, assuming that the extent of weathering in an individual sample is representative. Variability in hydrology and soil characteristics (e.g., 81) means that at field-scale, it is likely that multiple samples from sites representative of a range of field conditions (pH, density, etc.) will need to be analyzed for a representative weathering estimate to be calculated.

From the calculated *in-situ* cation-specific weathering rates of basalt feedstock, an initial rate of CDR (i.e. conversion of carbonic acid to bicarbonate) can be calculated, assuming the acidity consumed during silicate mineral dissolution is ultimately sourced from atmospheric CO₂ (see

Supporting Information Section 1.9 for more details). In many agricultural settings fertilizer amendments such as urea ammonium nitrate (UAN) are used. Nitrification of reduced nitrogen species is a source of strong acid that can also contribute to mineral weathering. In this case, feedstock weathering may or may not result in CDR. In cases where the strong acid would have interacted with a silicate mineral already, this weathering needs to be discounted from initial CDR estimates (see *Supporting Information Section 1.10*). The initial CDR rates calculated can be thought of as maximum possible CDR from an ERW deployment, and do not take into account downstream processes that will reduce the efficacy of carbon storage as bicarbonate in the river-ocean system, such as rerelease of CO₂ via the precipitation of secondary clays and carbonates outside the soil column, or potential degassing of CO₂ after conversion of bicarbonate to carbonic acid, from reequilibration in acidic solutions (e.g., 20, 63, 82-84).

2.2 Analytical requirements

Resolvability of a dissolution signal from soil-based mass-balance is a function of analytical uncertainty, feedstock application rate, and extent of feedstock dissolution. Limiting uncertainty on instrumentation used to analyze elemental composition is a critical aspect of the TiCAT approach — and is likely to be a critical issue for any other approach aiming to track CDR from the solid phase. This is due to the signal-to-noise ratio associated with measuring a small amount of feedstock mixed into a large amount of background soil. For technically and commercially feasible feedstock application rates (likely <50 t ha⁻¹, see 13), analytical uncertainty can result in overlap between error-bounded values for cation concentration of soil-feedstock mixtures before and after dissolution has occurred. Using representative soil and basalt compositions from this study for instance, at 5% analytical uncertainty (a typical lower bound for global analytical uncertainty in X-ray fluorescence measurements of major element concentration in soils, see e.g., 85-87, and *Supporting Information Section 1.7*) a 25% loss of major cations from the basalt portion of a soil-feedstock mixture is unresolvable even at an application rate of 100 t ha⁻¹, assuming the mixture is homogenized to a depth of 10cm (a common mixing regime for managed row crop systems). However, at 1% analytical uncertainty the same extent of cation loss is resolvable at ~25 t ha⁻¹ (**Fig. 2**). Thus, when accounting for a range of plausible dissolution and application rates, analytical error must generally be limited to ~1% for our mass balance method to be accurate and widely applicable, a standard that is more stringent than that currently achievable by most commercial inorganic elemental analysis, including commercial mass spectrometry (e.g., 88, 89).

We obtain the requisite analytical precision for applying the TiCAT method here using isotope dilution inductively coupled plasma mass spectrometry (ID-ICP-MS). Isotope dilution is a well-established analytical method where the concentration of an element in a sample can be measured from the known concentration of an element in a spike solution, and the ratios of two isotopes of the same element in the natural sample and the spike respectively (90-92). The amount of an element in the sample, n_{sam} , is given by:

$$[n]_{sam} = [n]_{spk} \frac{R_{spk} - R_{mix} \sum_i R_{i,sam}}{R_{mix} - R_{sam} \sum_i R_{i,spk}} \quad (4)$$

where R is the ratio of two isotopes, and $\sum_i R_i$ is the sum of ratios of all isotopes to a reference isotope (e.g., 90; see also 91, 92). We used an isotope spike ‘cocktail’, doped with isotopes of Mg,

Ti, and Ca found in lower abundance in natural samples (**Supplemental Fig. S5**). Isotope spikes were prepared from powders of spiked TiO₂, MgO and CaCO₃. The pure spike Ca carbonate powders were digested using HCl, and the Mg and Ti oxide using HNO₃+HCl+HF. Following the digest each spike solution was calibrated by measuring the relative concentration of Mg, Ca, and Ti isotopes on a Thermo Scientific Neptune Plus multicollector ICP-MS for ~48 hours. Estimates of the uncertainty on the spike determination were < 0.1 ‰ based on replicate analysis. Individual spike solutions were then used to make an isotope spike ‘cocktail’ solution containing Mg, Ca and Ti spikes. The ‘cocktail’ was added to each sample during the dissolution stage of sample preparation to ensure sample-spike equilibration.

Isotope dilution allows for sample-specific calculation of element concentrations, unlike a standard calibration curve method whereby standard solutions of known concentration are run to relate element intensities (in counts per second) to concentration. Isotope dilution therefore corrects for matrix effects, mass bias, and instrument drift, and thus improves both accuracy and precision of measured concentrations, significantly reducing global analytical uncertainty (**Fig. 3**; see also 93). In addition to an iCAP TQ ICP-MS used to run samples for this study, we analyzed certified reference materials (BHVO-2 basalt and SGR-1b shale) on other ICP-MS models in order to test the data quality achieved by a variety of widely available instruments (a Perkin Elmer NexION 5000 Multi-Quadropole ICP-MS and a Thermo Scientific ElementXR High Resolution Magnetic Sector ICP-MS). For sample runs on the iCAP TQ ICP-MS, we were able to achieve average analytical uncertainty on reference materials of 0.22% for Ti, 0.78% for Mg, 0.39% for Ca, and 0.58% for Na (not using isotope dilution), when calculating uncertainty as the mean difference of calculated to certified values (global analytical uncertainty); and 0.75% for Ti, 1.16% for Mg, 1.29% for Ca, and 2.54% for Na (not using isotope dilution), when calculating uncertainty by the standard deviation of measurements as a percentage of the mean. Our results show that isotope dilution allows for a level of measurement accuracy and precision on quadrupole ICP-MS instruments that would otherwise typically only be achievable with a magnetic sector instrument. Given its much lower cost and far greater availability, the ability to leverage quadrupole ICP-MS for rapid, high-throughput analyses may ultimately be a critical factor in making this MRV technique economically viable at scale.

2.3 Mesocosm ERW experiments

As an initial test of the TiCAT method we employed laboratory mesocosm ERW experiments, which allowed us to independently estimate ERW and CDR by measuring the concentration of reaction products in plant, soil exchangeable fraction and leachate solution pools (see 29, 31, 33, 50-54, 56, 59). Each mesocosm contained a single C4 cereal crop *Sorghum bicolor* plant (see 33) with two different fertilizer treatments: nitrogen-phosphorus-potassium (NPK) (n=14), or manure (n=14). To half of the columns for each fertilizer treatment a basalt feedstock was added equivalent to an application rate of 5 kg m⁻² (50 t ha⁻¹), mixed to a depth of 12cm, and left in a controlled environment for 235 days (for a detailed description of mesocosm design and construction, substrate and feedstock preparation and characterization, plant varieties and growth conditions, and irrigation regime, see *Supporting Information*).

Leachate was collected from mesocosms at six discrete leachate events, accounting for the entire leachate flux during the experiment. After 235 days, samples were taken from relevant chemical pools — the soil exchangeable fraction, the solid phase with the exchangeable fraction removed by leaching with ammonium acetate, and the plant material (comprising shoots, roots and seeds). Analysis of total inorganic carbon (TIC) did not show detectable increases in a subset of mesocosm soils tested before leaching with ammonium acetate (using an Eltra C/S Analyzer with detection limit of 0.1wt%), suggesting that carbonate formation should have a negligible impact on the overall cation budget of the mesocosm systems. Aliquots of solid phase samples were then ashed, digested using $\text{HNO}_3+\text{HCl}+\text{HF}$, and elemental concentrations measured using ID-ICP-MS (see *Supporting Information Section 1.7*). Using a conventional approach focused on reaction products, we calculated elemental budgets for major cations for each mesocosm from the dissolved or non-mineral-bound pools (leachate + soil exchangeable fraction + plant material) (see *Supporting Information Section 1.8*). We compared the elemental budgets calculated for basalt-amended mesocosms to a control mesocosm for each fertilizer treatment that had no basalt applied. Control mesocosms were selected as the control replicates for which the topsoil major element composition most closely matched the initial soil baseline. The excess Na^+ , Ca^{2+} , and Mg^{2+} in the elemental budget of basalt-amended mesocosms relative to the controls were assumed to represent reaction products of basalt dissolution. From the amounts of these cations we obtained initial ERW rates. Using a modified Steiour formulation – a simple stoichiometric approach that relates the amount of mobile cations to the amount of carbonic acidity converted to bicarbonate by charge balance (see *Supporting Information Section 1.3*) – ERW rates were converted to initial CDR estimates.

These rates can be compared with those obtained using the TiCAT method, as the cations released into non-mineral-bound pools from feedstock weathering should correspond to the amount of cation loss from the basalt fraction being weathered. We analyzed the concentration of Na, Ca, Mg and Ti in the solid phase samples taken from the upper 12cm portion of each mesocosm. We calculated F_D of the basalt fraction present in the soil + basalt mixture separately for each major cation, and corrected these for the concentration effect from basalt dissolution (see Section 2.1, also *Supporting Information Section 1.9*). From the corrected cation-specific F_D for each mesocosm and using the application rate of basalt for each mesocosm, we calculated the total amount of major cations in basalt applied over a given area that was dissolved (see *Supporting Information Section 1.9*), giving an initial ERW rate, and using the same modified Steiour formulation as above, an initial CDR estimate. To directly compare the TiCAT method to a weathering product approach, we applied a correction to the TiCAT estimates to account for strong acid weathering from nitrification of fertilizers (see *Supporting Information Section 1.10*).

3 Results and Discussion

Our results show agreement between two independent methods of calculating weathering and initial CDR in our mesocosm systems (**Fig. 4a**). The more conventional approach, measuring cation reaction products in dissolved cation pools, yielded mean initial CDR estimates of $1.68 \pm 0.11 \text{ tCO}_2\text{eq ha}^{-1}$ (NPK-fertilized) and $1.05 \pm 0.15 \text{ tCO}_2\text{eq ha}^{-1}$ (manure-fertilized) across all mesocosms. The TiCAT approach introduced here, which measures cation loss from the solid phase of soil samples, gave mean initial CDR estimates of $1.84 \pm 0.37 \text{ tCO}_2\text{eq ha}^{-1}$ (NPK-fertilized) and $1.04 \pm 0.37 \text{ tCO}_2\text{eq ha}^{-1}$ (manure-fertilized). Thus, mean initial CDR estimates from the TiCAT method were within (\pm standard error of means) of those from the reaction product method for both NPK- and manure-fertilized basalt-amended mesocosms.

Mean initial CDR values across all basalt-amended mesocosms were $1.44 \pm 0.27 \text{ tCO}_2\text{eq ha}^{-1}$ (TiCAT), and $1.36 \pm 0.12 \text{ tCO}_2\text{eq ha}^{-1}$ (dissolved pools) (**Fig. 4b**). This is broadly consistent with estimated CDR values calculated for similar ERW studies, albeit these range greatly in application amount and duration (see 34). Given a CDR potential for the basalt used in our study of $183.56 \text{ kgCO}_2 \text{ t}^{-1}$ (see *Supporting Information Section 1.3*), the initial CDR after 235 days of carbonic-acid-driven weathering was $15.7 \pm 3.1 \%$ of this potential, using results from TiCAT. Our results thus demonstrate that the solid-phase approach underlying TiCAT produces estimates for initial CDR within error of those calculated by analyzing the dissolved, plant, and soil exchangeable cation pools that constitute the ultimate reaction products in our mesocosm experiments, suggesting that it can yield an accurate and robust estimate of initial CDR in enhanced weathering systems.

It is important to emphasize that the CDR rate estimated based on the time-integrated amount of feedstock dissolution and cation loss should only be regarded as an initial CDR value. There is potential for leakage of initially captured carbon downstream of a given field deployment, as alkalinity and dissolved inorganic carbon are transported from the soil column to the oceans (e.g., 20, 63, 82-84). In addition, a large fraction of the dissolved cation load in any soil will be transiently hosted in soil exchange sites (e.g., 94-97; see also 56). This cation storage at exchange sites is temporary, and upon their release dissolved cations will drive CDR through charge balance in the carbonic acid system (see 51, 52). However, this means there is a variable lag time between feedstock dissolution and CO_2 capture that needs to be considered for accurate CDR quantification. Given these factors, a robust, “cradle-to-grave” MRV approach with TiCAT at its core will also require modeling the transport of weathering products through the soil (14, 19, 47, 98) and groundwater-river-ocean system (20, 82-84) to determine potential leakage through re-release of CO_2 back to the atmosphere. In the near term, developing and testing these models should be done in conjunction with monitoring of aqueous geochemistry, alongside soil-based approaches (such as TiCAT). As with all CDR techniques, emissions accounting must also be implemented to calculate net CDR rates.

There are several key challenges that need to be met before TiCAT can be widely applied. First of all, it must be demonstrated that scaling from weathering rates at specific sampling points to a larger system allows for a representative measurement of weathering across that system, while minimizing uncertainty. This study suggests that this condition can be met, at least when averaging across mesocosm experiments. Secondly, spatial heterogeneity of elemental concentrations in managed soils must be examined to assess the density and volume of sampling that must be implemented to be able to directly compare between samples of background soil before ERW feedstock amendment and post-amendment soil; in both cases, specific sampling protocols such as pooling and/or gridded sampling may be useful tools in making representative measurements (81), and control sites will be useful for testing these. A complication is that in open systems such as agricultural fields, material may be introduced from external sources that could interfere with the simple two-member mixing model (e.g. flooding events, windblown dust). Further, in some settings other soil amendments may be used in conjunction with silicate minerals. If these contain significant amounts of major cations, or the immobile tracer, a more elaborate mixing model must be used to account for these. Additionally, the TiCAT approach may not be viable as a standalone MRV framework in specific cases: for example in settings with very high physical erosion; in

settings where there is significant and fast weathering from soils; where feedstocks are used that have a very similar chemical composition to the soil or have lower concentrations of all immobile trace elements; or where feedstocks are especially slow-weathering, such as in arid settings not conducive to ERW. Other site-specific conditions may require alterations to workflows; for example, the depth of sampling required may vary in response to variable mixing depths, as modulated by tilling practices, crop type, and biological mixing.

Lastly, effective implementation of the TiCAT approach relies on stringent constraints on analytical error, which may be challenging via standard practice with most commercially available measurements for elemental concentration, including ICP-MS (see 88, 89). Nonetheless, here we have demonstrated that it is possible using isotope dilution on a standard quadrupole ICP-MS instrument to minimize analytical error to ~1%, making even <10% basalt dissolution analytically resolvable for total feedstock application rates of 50 t ha⁻¹. However, replication of this analytical precision in commercial laboratories will require adjustment to workflows and standard operating procedures. It is also likely that the aggregate impact on unit cost (dollar cost per ton of CO₂ captured) of TiCAT as an MRV procedure will broadly follow a “learning curve” trajectory, driving lower costs as ERW is scaled up (e.g., 99).

The TiCAT method overcomes some of the issues with prior methods of estimating ERW, particularly those that rely on accurately measuring the amount and transport of weathering reaction products (i.e., bicarbonate ions, HCO₃⁻, or cations in soil drainage waters) after feedstock application. Methods that rely on tracking the dissolved phase are extremely time- and labor-intensive, introducing significant barriers to scale. For example, a thorough study of a field-scale ERW trial monitoring aqueous reaction products, such as that conducted by ref. 59, involves many months of labor- and time-intensive sampling not only of soils, plants, and possibly porewaters from the agricultural plots onto which ERW feedstock is applied, but also a wider detailed monitoring of the drainage regime and watershed around such a site. Even using this style of sampling protocol, the necessary granularity of measurements would likely miss short-term fluctuations such as wash-out after rain events, which in many river systems account for an important component of the overall solute discharge (e.g., 100). Such measurements, as well as those reliant on directly measuring soil exchangeable cations, can also be complicated by varying timeframes over which cations are bound to exchangeable sorption sites within a soil (see 51, 52).

Our approach also directly overcomes possibly the largest uncertainty in scaling ERW in agricultural settings — estimating the initial extent of feedstock dissolution in soils (see e.g., 34; 61). There is currently significant uncertainty on how rock grain surface areas evolve through time within a given field setting (i.e., individual farm), and the extent to which secondary mineral formation on the surface of feedstock has the potential to alter mineral dissolution rates (e.g., 101-109). In addition, bulk mineral dissolution kinetics are in some cases poorly constrained (e.g., 105, 110, 111). Taken together, these considerations make it extremely challenging to accurately forecast feedstock dissolution across a range of deployment regimes with existing reactive transport models alone (34, 61, 101-111).

A significant additional advantage to this MRV approach is that it can directly integrate into existing agronomic practices. Samples from the uppermost portion of the soil are already regularly taken for nutrient and soil pH analysis (e.g., 94, 112). Importantly, this means that there is already

extensive personnel and infrastructure in place that can be leveraged to scale empirical validation of ERW at minimal cost, in marked contrast to empirical verification of soil organic carbon concentrations (SOC), which requires modified sampling protocols for accurate empirical results. Existing frameworks for carbon storage in agricultural settings are mostly focused on SOC, which does not allow for landowners and land users to include alkalinity generation through practices such as ERW into an estimate of carbon storage. Deployment of ERW at scale requires MRV tools such as TiCAT to be incorporated into these frameworks. This would allow for combined use of ERW and SOC maintenance to achieve maximum carbon storage depending on local conditions.

In summary, we have demonstrated with mesocosm ERW experiments that a soil-based mass balance approach — TiCAT — accurately tracks ERW with a basalt feedstock to allow estimation of CDR rates. TiCAT yields estimates that are within error of those calculated by complete elemental budgeting of weathering reaction products gained in plant and exchangeable cation pools. Using an isotope dilution method, we can reduce analytical error sufficiently that a dissolution signal is resolvable in the solid soil phase at reasonable feedstock application rates. Applying the methods used in this study to field-scale trials is a necessary next step in verifying the capacity of TiCAT to be used for MRV in ERW in the field. Additionally, our approach will ultimately need to be augmented by the development of cradle-to-grave MRV approaches that can provide error-bounded estimates of final CDR. Nevertheless, our results suggest that a soil-based mass-balance method could be a cost-effective and accurate centerpiece of a robust MRV toolkit for deploying ERW at scale.

Figures

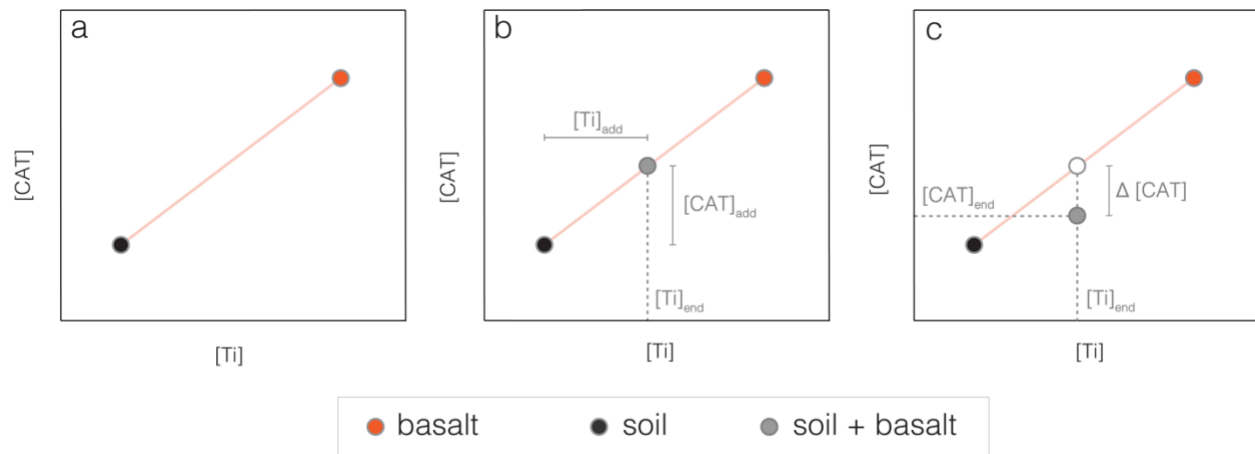


Fig. 1. The TiCAT conceptual framework as a simple two-component mixing model. Idealized soil and basalt (a commonly proposed ERW feedstock) endmember compositions are plotted in [Ti] v [CAT] space (a). A mixture of soil + basalt initially plots on the idealized mixing line between both endmembers (b). Dissolution results in loss of [CAT] from the solid phase, while [Ti] is conserved as it is immobile; the original composition of the soil + basalt mixture (indicated by the white circle) is the intersection of $[Ti]_{end}$ with the mixing line, and $\Delta [CAT]$ is the amount of CAT lost by dissolution (c).

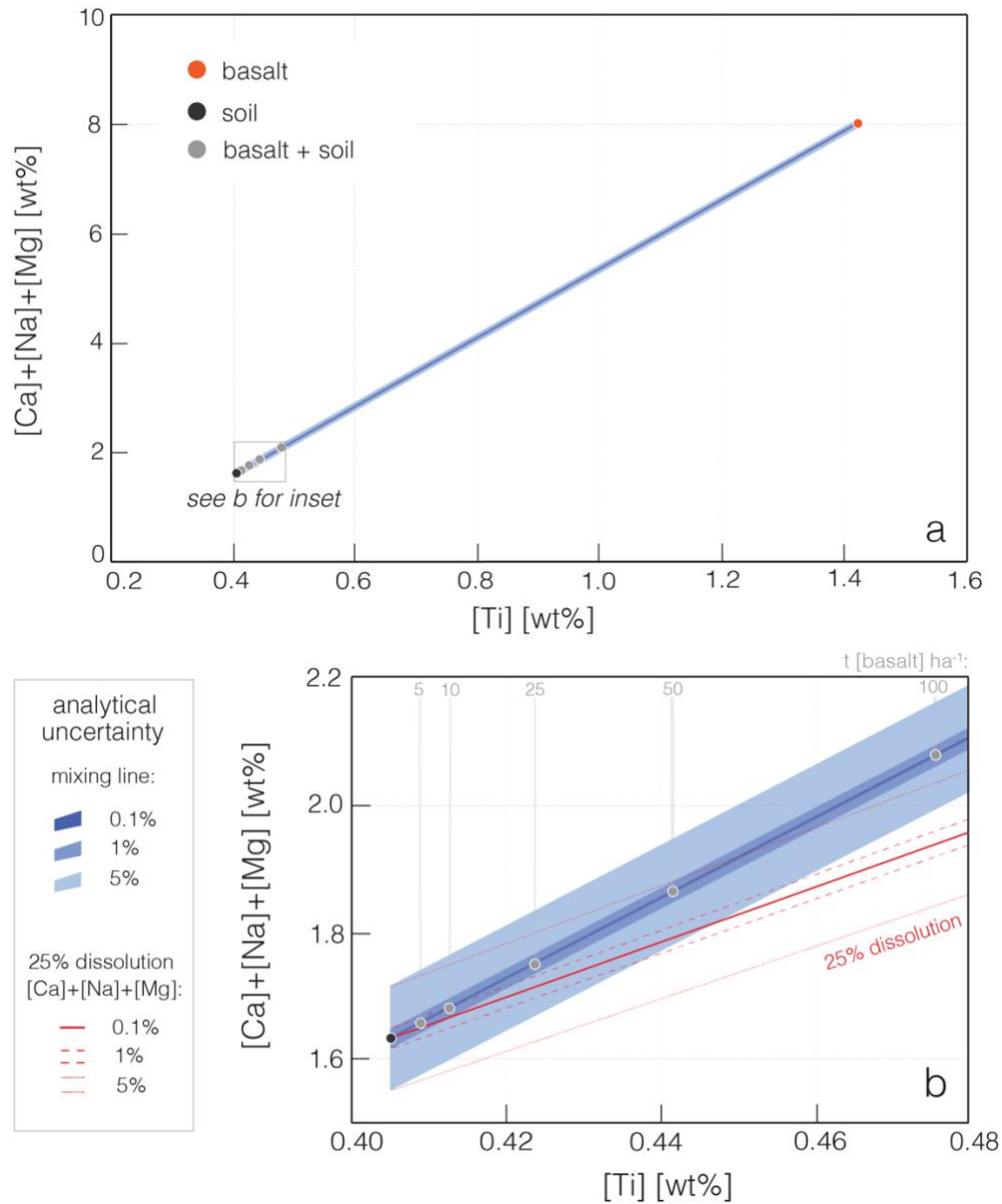


Fig. 2. A mixing model with representative data for soil and basalt feedstock endmembers. Assumed homogeneous mixtures of soil + basalt to 10cm mixing depth are shown for a range of basalt application scenarios (see inset, b). Error envelopes are shown for the mixing line and a line indicating theoretical 25% dissolution, based on uncertainty in measuring the elemental concentration of soil and soil + basalt samples. Resolvability of a dissolution signal is dependent on dissolution rate, basalt application rate, and analytical error. Mixing line error envelope assumes that absolute analytical error of basalt is same as soil, a realistic scenario given repeat measurements of a bulk feedstock; dissolution error envelope assumes that sampling gives a representative soil background.

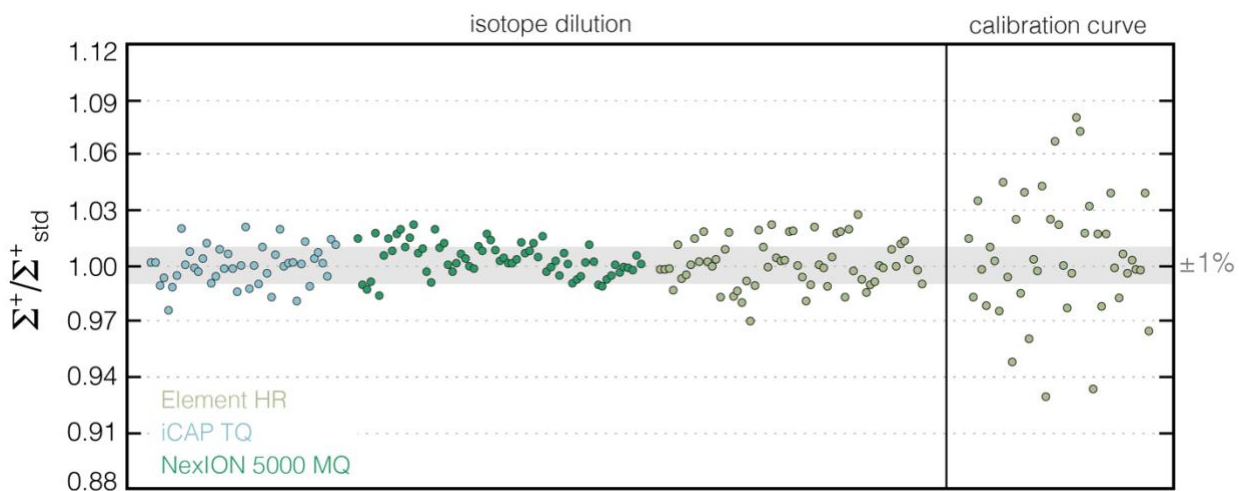


Fig 3. Representative analytical error for Ca, Mg, and Ti on standards run on three different ICP-MS instruments, using a calibration curve method and an isotope dilution method. Isotope dilution cannot be applied to Na as it has a single stable isotope. The grey shaded region represents an analytical error range of $\pm 1\%$. ICP-MS instruments used were two quadrupole instruments, a Thermo Scientific iCAP TQ ICP-MS and a Perkin Elmer NexION 5000 Multi-Quadropole ICP-MS; as well as a Thermo Scientific Element High Resolution Magnetic Sector ICP-MS.

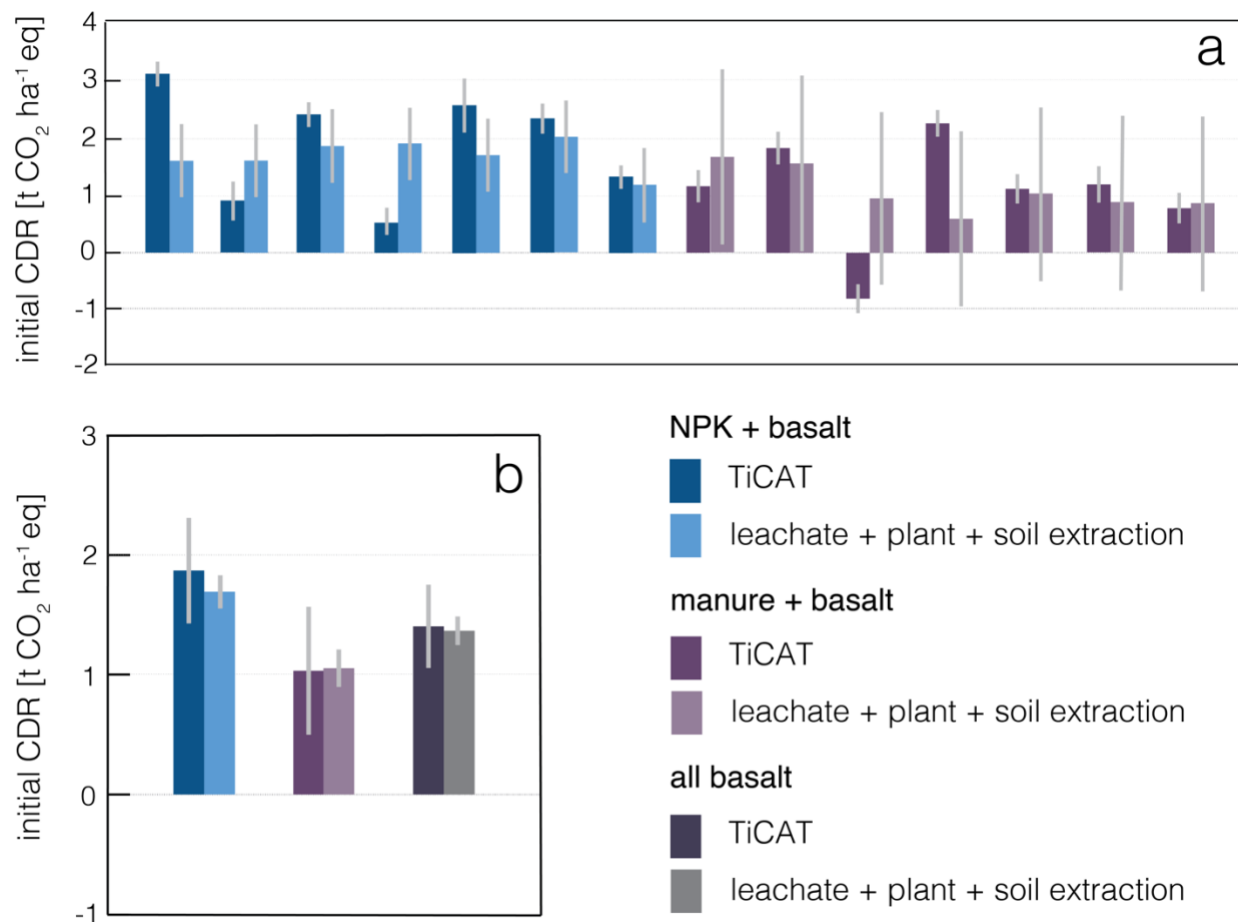


Fig 4. Initial CDR estimates calculated using cation data from TiCAT and from non-mineral-bound cation budgets. Results are shown for individual mesocosms (a), and as mean values for all mesocosms pooled by treatment type, where dark grey bars show all basalt-treated mesocosms as a single pooled data set (b). Error bars for TiCAT are propagated analytical error in (a), and standard error of means ($\pm \sigma$) where baseline soil and basalt samples have been pooled. Error bars for leachate + plant + soil extraction are propagated standard error between measurements for all mesocosms of the same treatment in (a), and standard error of means ($\pm \sigma$) where baseline soil and basalt samples have been pooled.

Supporting Information

Contains Supporting Materials and Methods (1.1-1.10), Supporting Tables (Tables S1-S2), Supporting Figures (Figures S1-S10), and Supporting References. Supporting Datasets and Software attached (Datasets S1-S3, Software S1).

Acknowledgments

We thank Dr Amy L. McBride for providing the basalt mineralogy and particle size distribution data for this study. We also acknowledge technical support from Irene Johnson and Dr Karen J. Bailey during soil excavation, plant tissue preparation and the ammonium acetate soil extraction. Six reviewers gave helpful and constructive feedback that improved this study. N.J.P. and T.J.S. acknowledge support from the Yale Center for Natural Carbon Capture. M.K. acknowledges funding through an NERC/ACCE DTP studentship and D.J.B. and D.Z.E acknowledge funding from the Leverhulme Trust through a Leverhulme Research Centre award (RC-2015-029).

References

1. Ou, Y.; Iyer, G.; Clarke, L.; Edmonds, J.; Fawcett, A.A.; Hultman, N.; McFarland, J.R.; Binsted, M.; Cui, R.; Fyson, C.; Geiges, A.; Gonzales-Zuñiga, S.; Gidden, M.J.; Höhne, N.; Jeffery, L.; Kuramochi, T.; Lewis, J.; Meinshausen, M.; Nicholls, Z.; Patel, P.; Ragnauth, S.; Rogelj, J.; Waldhoff, S.; Yu, S.; McJeon, H. Can updated climate pledges limit warming well below 2°C? *Science* **2021**, *374*, 693–695. <https://doi.org/10.1126/science.abl8976>
2. Meinshausen, M.; Lewis, J.; McGlade, C.; Gütschow, J.; Nicholls, Z.; Burdon, R.; Cozzi, L.; Hackmann, B. Realization of Paris Agreement pledges may limit warming just below 2 °C. *Nature* **2022**, *604*, 304–309. <https://doi.org/10.1038/s41586-022-04553-z>
3. United Nations Environment Programme. *Emissions Gap Report 2022: The Closing Window — Climate crisis calls for rapid transformation of societies*. **2022**. <https://www.unep.org/emissions-gap-report-2022>
4. Lawrence, M.G.; Schäfer, S.; Muri, H.; Scott, V.; Oschlies, A.; Vaughan, N.E.; Boucher, O.; Schmidt, H.; Haywood, J.; Scheffran, J. Evaluating climate geoengineering proposals in the context of the Paris Agreement temperature goals. *Nat Commun* **2018**, *9*, 3734. <https://doi.org/10.1038/s41467-018-05938-3>
5. Intergovernmental Panel on Climate Change. *Climate Change 2022: Mitigation of Climate Change. Contribution of Working Group III to the Sixth Assessment Report of the Intergovernmental Panel on Climate Change*; P.R. Shukla, J. Skea, R. Slade, A. Al Khourdajie, R. van Diemen, D. McCollum, M. Pathak, S. Some, P. Vyas, R. Fradera, M. Belkacemi, A. Hasija, G. Lisboa, S. Luz, J. Malley, Eds.; Cambridge University Press, **2022**, doi: 10.1017/9781009157926
6. Schuiling, R.D.; Krijgsman, P. Enhanced Weathering: An Effective and Cheap Tool to Sequester Co₂. *Climatic Change*, **2006**, *74*, 349–354. <https://doi.org/10.1007/s10584-005-3485-y>
7. Köhler, P.; Hartmann, J.; Wolf-Gladrow, D.A. Geoengineering potential of artificially enhanced silicate weathering of olivine. *Proc National Acad Sci*, **2010**, *107*, 20228–20233. <https://doi.org/10.1073/pnas.1000545107>
8. Renforth, P. The potential of enhanced weathering in the UK. *Int J Greenh Gas Con* **2012**, *10*, 229–243. <https://doi.org/10.1016/j.ijggc.2012.06.011>
9. Hartmann, J.; West, A.J.; Renforth, P.; Köhler, P.; Rocha, C.L.D.L.; Wolf-Gladrow, D.A.; Dürr, H.H.; Scheffran, J. Enhanced chemical weathering as a geoengineering strategy to reduce atmospheric carbon dioxide, supply nutrients, and mitigate ocean acidification. *Rev Geophys*, **2013**, *51*, 113–149. <https://doi.org/10.1002/rog.20004>
10. Kantola, I.B.; Masters, M.D.; Beerling, D.J.; Long, S.P.; DeLucia, E.H. Potential of global croplands and bioenergy crops for climate change mitigation through deployment for enhanced weathering. *Biol Letters*, **2017**, *13*, 20160714. <https://doi.org/10.1098/rsbl.2016.0714>
11. Taylor, L.L.; Beerling, D.J.; Quegan, S.; Banwart, S.A. Simulating carbon capture by enhanced weathering with croplands: an overview of key processes highlighting areas of future model development. *Biol Letters*, **2017**, *13*, 20160868. <https://doi.org/10.1098/rsbl.2016.0868>
12. Strefler, J.; Amann, T.; Bauer, N.; Kriegler, E.; Hartmann, J. Potential and costs of carbon dioxide removal by enhanced weathering of rocks. *Environ Res Lett*, **2018**, *13*, 034010. <https://doi.org/10.1088/1748-9326/aaa9c4>

13. Beerling, D.J.; Leake, J.R.; Long, S.P.; Scholes, J.D.; Ton, J.; Nelson, P.N.; Bird, M.; Kantzas, E.; Taylor, L.L.; Sarkar, B.; Kelland, M.; DeLucia, E.; Kantola, I.; Müller, C.; Rau, G.; Hansen, J. Farming with crops and rocks to address global climate, food and soil security. *Nat Plants*, **2018**, *4*, 138–147. <https://doi.org/10.1038/s41477-018-0108-y>
14. Beerling, D.J.; Kantzas, E.P.; Lomas, M.R.; Wade, P.; Eufrazio, R.M.; Renforth, P.; Sarkar, B.; Andrews, M.G.; James, R.H.; Pearce, C.R.; Mercure, J.-F.; Pollitt, H.; Holden, P.B.; Edwards, N.R.; Khanna, M.; Koh, L.; Quegan, S.; Pidgeon, N.F.; Janssens, I.A.; Hansen, J.; Banwart, S.A. Potential for large-scale CO₂ removal via enhanced rock weathering with croplands. *Nature*, **2020**, *583*, 242–248. <https://doi.org/10.1038/s41586-020-2448-9>
15. Taylor, L.L.; Quirk, J.; Thorley, R.M.S.; Kharecha, P.A.; Hansen, J.; Ridgwell, A.; Lomas, M.R.; Banwart, S.A.; Beerling, D.J. Enhanced weathering strategies for stabilizing climate and averting ocean acidification. *Nat Clim Change*, **2016**, *6*, 402–406. <https://doi.org/10.1038/nclimate2882>
16. Edwards, D.P.; Lim, F.; James, R.H.; Pearce, C.R.; Scholes, J.; Freckleton, R.P.; Beerling, D.J. Climate change mitigation: potential benefits and pitfalls of enhanced rock weathering in tropical agriculture. *Biol Letters*, **2017**, *13*, 20160715. <https://doi.org/10.1098/rsbl.2016.0715>
17. Goll, D.S.; Ciais, P.; Amann, T.; Buermann, W.; Chang, J.; Eker, S.; Hartmann, J.; Janssens, I.; Li, W.; Obersteiner, M.; Penuelas, J.; Tanaka, K.; Vicca, S. Potential CO₂ removal from enhanced weathering by ecosystem responses to powdered rock. *Nat Geosci*, **2021**, *14*, 545–549. <https://doi.org/10.1038/s41561-021-00798-x>
18. Rinder, T.; von Hagke, C. The influence of particle size on the potential of enhanced basalt weathering for carbon dioxide removal - Insights from a regional assessment. *J Clean Prod*, **2021**, *315*, 128178. <https://doi.org/10.1016/j.jclepro.2021.128178>
19. Kantzas, E.P.; Martin, M.V.; Lomas, M.R.; Eufrazio, R.M.; Renforth, P.; Lewis, A.L.; Taylor, L.L.; Mecure, J.-F.; Pollitt, H.; Vercoulen, P.V.; Vakilifard, N.; Holden, P.B.; Edwards, N.R.; Koh, L.; Pidgeon, N.F.; Banwart, S.A.; Beerling, D.J. Substantial carbon drawdown potential from enhanced rock weathering in the United Kingdom. *Nat Geosci*, **2022**, *15*, 382–389. <https://doi.org/10.1038/s41561-022-00925-2>
20. Zhang, S.; Planavsky, N.J.; Katchinoff, J.; Raymond, P.A.; Kanzaki, Y.; Reershemius, T.; Reinhard, C.T. River chemistry constraints on the carbon capture potential of surficial enhanced rock weathering. *Limnol Oceanogr*, **2022**, <https://doi.org/10.1002/lno.12244>
21. Haque, F.; Khalidy, R.; Chiang, Y. W.; Santos, R. M. Constraining the Capacity of Global Croplands to CO₂ Drawdown via Mineral Weathering. *ACS Earth Space Chem*. **2023**. <https://doi.org/10.1021/acsearthspacechem.2c00374>.
22. Middelburg, J. J.; Soetaert, K.; Hagens, M. Ocean Alkalinity, Buffering and Biogeochemical Processes. *Reviews of Geophysics*, **2020.**, *58*(3), e2019RG000681. <https://doi.org/10.1029/2019rg000681>
23. Urey, H. C. On the Early Chemical History of the Earth and the Origin of Life. *Proceedings of the National Academy of Sciences*, **1952**, *38*(4), 351–363. <https://doi.org/10.1073/pnas.38.4.351>
24. Berner, R. A.; Lasaga, A. C.; Garrels, R. M. The carbonate-silicate geochemical cycle and its effect on atmospheric carbon dioxide over the past 100 million years. *American Journal of Science*, **1983**, *283*(7), 641–683. <https://doi.org/10.2475/ajs.283.7.641>

25. Isson, T. T.; Planavsky, N. J.; Coogan, L. A.; Stewart, E. M.; Ague, J. J.; Bolton, E. W.; Zhang, S.; McKenzie, N. R.; Kump, L. R. Evolution of the Global Carbon Cycle and Climate Regulation on Earth. *Global Biogeochemical Cycles*, **2020**, *34*(2). <https://doi.org/10.1029/2018gb006061>
26. Smith, P. Soil carbon sequestration and biochar as negative emission technologies. *Global Change Biol*, **2016**, *22*, 1315–1324. <https://doi.org/10.1111/gcb.13178>
27. Schlesinger, W.H.; Amundson, R. Managing for soil carbon sequestration: Let's get realistic. *Global Change Biol*, **2019**, *25*, 386–389. <https://doi.org/10.1111/gcb.14478>
28. Bossio, D.A.; Cook-Patton, S.C.; Ellis, P.W.; Fargione, J.; Sanderman, J.; Smith, P.; Wood, S.; Zomer, R.J.; von Unger, M.; Emmer, I.M.; Griscom, B.W. The role of soil carbon in natural climate solutions. *Nat Sustain*, **2020**, *3*, 391–398. <https://doi.org/10.1038/s41893-020-0491-z>
29. ten Berge, H.F.M.; van der Meer, H.G.; Steenhuizen, J.W.; Goedhart, P.W.; Knops, P.; Verhagen, J. Olivine Weathering in Soil, and Its Effects on Growth and Nutrient Uptake in Ryegrass (*Lolium perenne* L.): A Pot Experiment. *Plos One*, **2012**, *7*, e42098. <https://doi.org/10.1371/journal.pone.0042098>
30. Song, Z.; Liu, C.; Müller, K.; Yang, X.; Wu, Y.; Wang, H. Silicon regulation of soil organic carbon stabilization and its potential to mitigate climate change. *Earth-sci Rev* **2018**, *185*, 463–475. <https://doi.org/10.1016/j.earscirev.2018.06.020>
31. Amann, T.; Hartmann, J.; Struyf, E.; Garcia, W. de O.; Fischer, E.K.; Janssens, I.; Meire, P.; Schoelynck, J. Enhanced Weathering and related element fluxes – a cropland mesocosm approach. *Biogeosciences*, **2020**, *17*, 103–119. <https://doi.org/10.5194/bg-17-103-2020>
32. Garcia, W. de O.; Amann, T.; Hartmann, J.; Karstens, K.; Popp, A.; Boysen, L.R.; Smith, P.; Goll, D. Impacts of enhanced weathering on biomass production for negative emission technologies and soil hydrology. *Biogeosciences*, **2020**, *17*, 2107–2133. <https://doi.org/10.5194/bg-17-2107-2020>
33. Kelland, M.E.; Wade, P.W.; Lewis, A.L.; Taylor, L.L.; Sarkar, B.; Andrews, M.G.; Lomas, M.R.; Cotton, T.E.A.; Kemp, S.J.; James, R.H.; Pearce, C.R.; Hartley, S.E.; Hodson, M.E.; Leake, J.R.; Banwart, S.A.; Beerling, D.J. Increased yield and CO₂ sequestration potential with the C₄ cereal *Sorghum bicolor* cultivated in basaltic rock dust-amended agricultural soil. *Global Change Biol*, **2020**, *26*, 3658–3676. <https://doi.org/10.1111/gcb.15089>
34. Swoboda, P.; Döring, T.F.; Hamer, M. Remineralizing soils? The agricultural usage of silicate rock powders: A review. *Sci Total Environ*, **2021**, *807*, 150976. <https://doi.org/10.1016/j.scitotenv.2021.150976>
35. Guo, F.; Wang, Y.; Zhu, H.; Zhang, C.; Sun, H.; Fang, Z.; Yang, J.; Zhang, L.; Mu, Y.; Man, Y. B.; Wu, F. Crop Productivity and Soil Inorganic Carbon Change Mediated by Enhanced Rock Weathering in Farmland: A Comparative Field Analysis of Multi-Agroclimatic Regions in Central China. *Agric. Syst.* **2023**, *210*, 103691. <https://doi.org/10.1016/j.agsy.2023.103691>.
36. Luchese, A. V.; Leite, I. J. G. de C.; Alves, M. L.; Vieceli, J. P. dos S.; Pivetta, L. A.; Missio, R. F. Can Basalt Rock Powder Be Used as an Alternative Nutrient Source for Soybeans and Corn? *J. Soil Sci. Plant Nutr.* **2023**, 1–11. <https://doi.org/10.1007/s42729-023-01322-3>.

37. Reynaert, S.; Vienne, A.; Boeck, H. J. D.; D'Hose, T.; Janssens, I.; Nijs, I.; Portillo-Estrada, M.; Verbruggen, E.; Vicca, S.; Poblador, S. Basalt Addition Improves the Performance of Young Grassland Monocultures under More Persistent Weather Featuring Longer Dry and Wet Spells. *Agric. For. Meteorol.* **2023**, *340*, 109610. <https://doi.org/10.1016/j.agrformet.2023.109610>.
38. Davies, B.; Finney, B.; Eagle, D. *Resource Management: Soil*. Farming Press, **2001**, ISBN 0 85236 559 4.
39. Kamprath, E.J.; Smyth, T.J. Liming. In: *Encyclopedia of Soils in the Environment*; Hillel, D. Ed.; Elsevier, **2005** ISBN 9780123485304, 350-358, <https://doi.org/10.1016/B0-12-348530-4/00225-3>
40. Goulding, K.W.T. Soil acidification and the importance of liming agricultural soils with particular reference to the United Kingdom. *Soil Use Manage*, **2016**, *32*: 390-399. <https://doi.org/10.1111/sum.12270>
41. Semhi, K.; Suchet, P.A.; Clauer, N.; Probst, J.-L. Impact of nitrogen fertilizers on the natural weathering-erosion processes and fluvial transport in the Garonne basin. *Appl Geochem*, **2000**, *15*, 865–878. [https://doi.org/10.1016/s0883-2927\(99\)00076-1](https://doi.org/10.1016/s0883-2927(99)00076-1)
42. West, T.O.; McBride, A.C. The contribution of agricultural lime to carbon dioxide emissions in the United States: dissolution, transport, and net emissions. *Agric Ecosyst Environ*, **2005**, *108*, 145–154. <https://doi.org/10.1016/j.agee.2005.01.002>
43. Oh, N.; Raymond, P.A. Contribution of agricultural liming to riverine bicarbonate export and CO₂ sequestration in the Ohio River basin. *Global Biogeochem Cy*, **2006**, *20*, n/a-n/a. <https://doi.org/10.1029/2005gb002565>
44. Hamilton, S.K.; Kurzman, A.L.; Arango, C.; Jin, L.; Robertson, G.P. Evidence for carbon sequestration by agricultural liming. *Global Biogeochem Cy*, **2007**, *21*, n/a-n/a. <https://doi.org/10.1029/2006gb002738>
45. Perrin, A.-S.; Probst, A.; Probst, J.-L. Impact of nitrogenous fertilizers on carbonate dissolution in small agricultural catchments: Implications for weathering CO₂ uptake at regional and global scales. *Geochim Cosmochim Acta*, **2008**, *72*, 3105–3123. <https://doi.org/10.1016/j.gca.2008.04.011>
46. Dietzen, C.; Harrison, R.; Michelsen-Correa, S. Effectiveness of enhanced mineral weathering as a carbon sequestration tool and alternative to agricultural lime: An incubation experiment. *Int J Greenh Gas Con*, **2018**, *74*, 251–258. <https://doi.org/10.1016/j.ijggc.2018.05.007>
47. Kanzaki, Y.; Zhang, S.; Planavsky, N.J.; Reinhard, C.T. Soil Cycles of Elements simulator for Predicting TERrestrial regulation of greenhouse gases: SCEPTER v0.9. *Geoscientific Model Dev Discuss*, **2022**, 1–58. <https://doi.org/10.5194/gmd-2022-8>
48. Deng, H.; Sonnenthal, E.; Arora, B.; Breunig, H.; Brodie, E.; Kleber, M.; Spycher, N.; Nico, P. The Environmental Controls on Efficiency of Enhanced Rock Weathering in Soils. *Sci. Rep.* **2023**, *13* (1), 9765. <https://doi.org/10.1038/s41598-023-36113-4>.
49. Cipolla, G.; Calabrese, S.; Noto, L.V.; Porporato, A. The role of hydrology on enhanced weathering for carbon sequestration I. Modeling rock-dissolution reactions coupled to plant, soil moisture, and carbon dynamics. *Adv Water Resour*, **2021**, *154*, 103934. <https://doi.org/10.1016/j.advwatres.2021.103934>
50. Renforth, P.; Pogge von Strandmann, P.A.E.; Henderson, G.M. The dissolution of olivine added to soil: Implications for enhanced weathering. *Appl Geochem*, **2015**, *61*, 109–118. <https://doi.org/10.1016/j.apgeochem.2015.05.016>

51. Pogge von Strandmann, P.A.E.; Fraser, W.T.; Hammond, S.J.; Tarbuck, G.; Wood, I.G.; Oelkers, E.H.; Murphy, M.J. Experimental determination of Li isotope behaviour during basalt weathering. *Chem Geol*, **2019**, *517*, 34–43. <https://doi.org/10.1016/j.chemgeo.2019.04.020>
52. Pogge von Strandmann, P.A.E.; Renforth, P.; West, A.J.; Murphy, M.J.; Luu, T.-H.; Henderson, G.M. The lithium and magnesium isotope signature of olivine dissolution in soil experiments. *Chem Geol*, **2021**, *560*, 120008. <https://doi.org/10.1016/j.chemgeo.2020.120008>
53. Pogge von Strandmann, P.A.E.; Tooley, C.; Mulders, J.J.P.A.; Renforth, P. The Dissolution of Olivine Added to Soil at 4°C: Implications for Enhanced Weathering in Cold Regions. *Frontiers Clim*, **2022**, *4*. <https://doi.org/10.3389/fclim.2022.827698>
54. Amann, T.; Hartmann, J.; Hellmann, R.; Pedrosa, E.T.; Malik, A. Enhanced weathering potentials—the role of in situ CO₂ and grain size distribution. *Frontiers Clim*, **2022**, *4*, 929268. <https://doi.org/10.3389/fclim.2022.929268>
55. Jariwala, H.; Haque, F.; Vanderburgt, S.; Santos, R.M.; Chiang, Y.W. Mineral–Soil–Plant–Nutrient Synergisms of Enhanced Weathering for Agriculture: Short-Term Investigations Using Fast-Weathering Wollastonite Skarn. *Front Plant Sci*, **2022**, *13*, 929457. <https://doi.org/10.3389/fpls.2022.929457>
56. Vienne, A.; Poblador, S.; Portillo-Estrada, M.; Hartmann, J.; Ijehon, S.; Wade, P.; Vicca, S. Enhanced Weathering Using Basalt Rock Powder: Carbon Sequestration, Co-benefits and Risks in a Mesocosm Study With *Solanum tuberosum*. *Frontiers Clim*, **2022**, *4*, 869456. <https://doi.org/10.3389/fclim.2022.869456>
57. Haque, F.; Santos, R.M.; Chiang, Y.W. CO₂ sequestration by wollastonite-amended agricultural soils – An Ontario field study. *Int J Greenh Gas Con*, **2020**, *97*, 103017. <https://doi.org/10.1016/j.ijggc.2020.103017>
58. Taylor, L.L.; Driscoll, C.T.; Groffman, P.M.; Rau, G.H.; Blum, J.D.; Beerling, D.J. Increased carbon capture by a silicate-treated forested watershed affected by acid deposition. *Biogeoscience*, **2021**, *18*, 169–188. <https://doi.org/10.5194/bg-18-169-2021>
59. Larkin, C.S.; Andrews, M.G.; Pearce, C.R.; Yeong, K.L.; Beerling, D.J.; Bellamy, J.; Benedick, S.; Freckleton, R.P.; Goring-Harford, H.; Sadekar, S.; James, R.H. Quantification of CO₂ removal in a large-scale enhanced weathering field trial on an oil palm plantation in Sabah, Malaysia. *Frontiers Clim*, **2022**, *4*, 959229. <https://doi.org/10.3389/fclim.2022.959229>
60. Dietzen, C.; Rosing, M. T. Quantification of CO₂ Uptake by Enhanced Weathering of Silicate Minerals Applied to Acidic Soils. *Int J Greenh Gas Con* **2023**, *125*, 103872. <https://doi.org/10.1016/j.ijggc.2023.103872>
61. Calabrese, S.; Wild, B.; Bertagni, M.B.; Bourg, I.C.; White, C.; Aburto, F.; Cipolla, G.; Noto, L.V.; Porporato, A. Nano- to Global-Scale Uncertainties in Terrestrial Enhanced Weathering. *Environ Sci Technol*, **2022**, <https://doi.org/10.1021/acs.est.2c03163>
62. Almaraz, M.; Bingham, N.L.; Holzer, I.O.; Geoghegan, E.K.; Goertzen, H.; Sohng, J.; Houlton, B.Z. Methods for determining the CO₂ removal capacity of enhanced weathering in agronomic settings. *Frontiers Clim*, **2022**, *4*, 970429. <https://doi.org/10.3389/fclim.2022.970429>
63. Chay, F.; Klitzke, J.; Hausfather, Z.; Martin, K.; Freeman, J.; Cullenward, D. 2022. Verification Confidence Levels for carbon dioxide removal. CarbonPlan <https://carbonplan.org/research/cdr-verification-explainer> (accessed 2023-05-08).

64. Knapp, W. J.; Stevenson, E. I.; Renforth, P.; Ascough, P. L.; Knight, A. C. G.; Bridgestock, L.; Bickle, M. J.; Lin, Y.; Riley, A. L.; Mayes, W. M.; Tipper, E. T. Quantifying CO₂ Removal at Enhanced Weathering Sites: A Multiproxy Approach. *Environ. Sci. Technol.* **2023**, *57* (26), 9854–9864. <https://doi.org/10.1021/acs.est.3c03757>.
65. Amann, T.; Hartmann, J. Carbon Accounting for Enhanced Weathering. *Frontiers Clim* **2022**, *4*, 849948. <https://doi.org/10.3389/fclim.2022.849948>.
66. Corwin, D. L.; Lesch, S. M. Apparent Soil Electrical Conductivity Measurements in Agriculture. *Comput Electron Agr* **2005**, *46* (1–3), 11–43. <https://doi.org/10.1016/j.compag.2004.10.005>.
67. Brimhall, G.H.; Dietrich, W.E. Constitutive mass balance relations between chemical composition, volume, density, porosity, and strain in metasomatic hydrochemical systems: Results on weathering and pedogenesis. *Geochim Cosmochim Acta*, **1987**, *51*, 567–587. [https://doi.org/10.1016/0016-7037\(87\)90070-6](https://doi.org/10.1016/0016-7037(87)90070-6)
68. Chadwick, O.A.; Brimhall, G.H.; Hendricks, D.M. From a black to a gray box — a mass balance interpretation of pedogenesis. *Geomorphology*, **1990**, *3*, 369–390. [https://doi.org/10.1016/0169-555x\(90\)90012-f](https://doi.org/10.1016/0169-555x(90)90012-f)
69. Chadwick, O.A.; Derry, L.A.; Vitousek, P.M.; Huebert, B.J.; Hedin, L.O. Changing sources of nutrients during four million years of ecosystem development. *Nature*, **1999**, *397*, 491–497. <https://doi.org/10.1038/17276>
70. Brimhall, G.H.; Lewis, C.J.; Ford, C.; Bratt, J.; Taylor, G.; Warin, O. Quantitative geochemical approach to pedogenesis: importance of parent material reduction, volumetric expansion, and eolian influx in lateritization. *Geoderma*, **1991**, *51*, 51–91. [https://doi.org/10.1016/0016-7061\(91\)90066-3](https://doi.org/10.1016/0016-7061(91)90066-3)
71. Kurtz, A.C.; Derry, L.A.; Chadwick, O.A.; Alfano, M.J. Refractory element mobility in volcanic soils. *Geology*, **2000**, *28*, 683–686. [https://doi.org/10.1130/0091-7613\(2000\)28<683:remivs>2.0.co;2](https://doi.org/10.1130/0091-7613(2000)28<683:remivs>2.0.co;2)
72. White, A.F.; Bullen, T.D.; Schulz, M.S.; Blum, A.E.; Huntington, T.G.; Peters, N.E. Differential rates of feldspar weathering in granitic regoliths. *Geochim Cosmochim Acta* **2001**, *65*, 847–869. [https://doi.org/10.1016/s0016-7037\(00\)00577-9](https://doi.org/10.1016/s0016-7037(00)00577-9)
73. Anderson, S.P.; Dietrich, W.E.; Brimhall, G.H. Weathering profiles, mass-balance analysis, and rates of solute loss: Linkages between weathering and erosion in a small, steep catchment. *GSA Bulletin*, **2002**, *114*, 1143–1158. [https://doi.org/10.1130/0016-7606\(2002\)114<1143:wpmbaa>2.0.co;2](https://doi.org/10.1130/0016-7606(2002)114<1143:wpmbaa>2.0.co;2)
74. Riebe, C.S.; Kirchner, J.W.; Finkel, R.C. Long-term rates of chemical weathering and physical erosion from cosmogenic nuclides and geochemical mass balance. *Geochim Cosmochim Acta*, **2003**, *67*, 4411–4427. [https://doi.org/10.1016/s0016-7037\(03\)00382-x](https://doi.org/10.1016/s0016-7037(03)00382-x)
75. Tabor, N.J.; Montañez, I.P.; Zierenberg, R.; Currie, B.S. Mineralogical and geochemical evolution of a basalt-hosted fossil soil (Late Triassic, Ischigualasto Formation, northwest Argentina): Potential for paleoenvironmental reconstruction. *GSA Bulletin*, **2004**, *116*, 1280–1293. <https://doi.org/10.1130/b25222.1>
76. Sheldon, N.D.; Tabor, N.J. Quantitative paleoenvironmental and paleoclimatic reconstruction using paleosols. *Earth-sci Rev*, **2009**, *95*, 1–52. <https://doi.org/10.1016/j.earscirev.2009.03.004>
77. Brantley, S.L.; Lebedeva, M. Learning to Read the Chemistry of Regolith to Understand the Critical Zone. *Annu Rev Earth Pl Sc*, **2011**, *39*, 387–416. <https://doi.org/10.1146/annurev-earth-040809-152321>

78. Fisher, B.A.; Rendahl, A.K.; Aufdenkampe, A.K.; Yoo, K. Quantifying weathering on variable rocks, an extension of geochemical mass balance: Critical zone and landscape evolution. *Earth Surf. Process. Landforms*, **2017**, *42*, 2457–2468. <https://doi.org/10.1002/esp.4212>
79. Lipp, A.G.; Shorttle, O.; Sperling, E.A.; Brocks, J.J.; Cole, D.B.; Crockford, P.W.; Mouro, L.D.; Dewing, K.; Dornbos, S.Q.; Emmings, J.F.; Farrell, U.C.; Jarrett, A.; Johnson, B.W.; Kabanov, P.; Keller, C.B.; Kunzmann, M.; Miller, A.J.; Mills, N.T.; O’Connell, B.; Peters, S.E.; Planavsky, N.J.; Ritzer, S.R.; Schoepfer, S.D.; Wilby, P.R.; Yang, J. The composition and weathering of the continents over geologic time. *Geochem Perspectives Lett*, **2021**, 21–26. <https://doi.org/10.7185/geochemlet.2109>
80. Middelburg, J.J.; van der Weijden, C.H.; Woittiez, J.R.W. Chemical processes affecting the mobility of major, minor and trace elements during weathering of granitic rocks. *Chem Geol*, **1988**, *68*, 253–273. [https://doi.org/10.1016/0009-2541\(88\)90025-3](https://doi.org/10.1016/0009-2541(88)90025-3)
81. Pennock, D.; Yates, T.; Braidek, J. Soil Sampling Designs. In: *Soil Sampling and Methods of Analysis*. Carter, M.R.; Gregorich, E.G.; eds. CRC Press, Canadian Society of Soil Science, **2008**, 23-38.
82. Knapp, W. J.; Tipper, E. T. The Efficacy of Enhancing Carbonate Weathering for Carbon Dioxide Sequestration. *Frontiers Clim* **2022**, *4*, 928215. <https://doi.org/10.3389/fclim.2022.928215>.
83. Harrington, K. J.; Hilton, R. G.; Henderson, G. M. Implications of the Riverine Response to Enhanced Weathering for CO₂ Removal in the UK. *Appl Geochem* **2023**, *152*, 105643. <https://doi.org/10.1016/j.apgeochem.2023.105643>.
84. Kanzaki, Y.; Planavsky, N. J.; Reinhard, C. T. New Estimates of the Storage Permanence and Ocean Co-Benefits of Enhanced Rock Weathering. *PNAS Nexus* **2023**, *2* (4), pgad059. <https://doi.org/10.1093/pnasnexus/pgad059>.
85. Rousseau, R. M. Detection Limit and Estimate of Uncertainty of Analytical XRF Results. *Rigaku J.* **2001**, *18* (2), 33-47.
86. Krishna, A. K.; Murthy, N. N.; Govil, P. K. Multielement Analysis of Soils by Wavelength-Dispersive X-Ray Fluorescence Spectrometry. *Atom. Spectrosc.* **2007**, *28* (6), 202-214.
87. Kenna, T. C.; Nitsche, F. O.; Herron, M. M.; Mailloux, B. J.; Peteet, D.; Sritrairat, S.; Sands, E.; Baumgarten, J. Evaluation and Calibration of a Field Portable X-Ray Fluorescence Spectrometer for Quantitative Analysis of Siliciclastic Soils and Sediments. *J. Anal. At. Spectrom.* **2010**, *26* (2), 395–405. <https://doi.org/10.1039/c0ja00133c>.
88. Andersen, J.E.T. On the development of quality assurance. *Trac Trends Anal Chem*, **2014**, *60*, 16–24. <https://doi.org/10.1016/j.trac.2014.04.016>
89. Eggen, O.A.; Reimann, C.; Flem, B. Reliability of geochemical analyses: Deja vu all over again. *Sci Total Environ*, **2019**, *670*, 138–148. <https://doi.org/10.1016/j.scitotenv.2019.03.185>
90. Inghram, M.G. Stable isotope dilution as an analytical tool. *Ann Rev Nucl Sci*, **1954**, *4*:1, 81-92. <https://doi.org/10.1146/annurev.ns.04.120154.000501>
91. Evans, E.H.; Clough, R. Isotope dilution analysis. In: *Encyclopedia of Analytical Science*, 2nd ed; Worsfold, P.; Townshend, A.; Poole., C.; Eds.. Elsevier, **2005**, 545-553. <https://doi.org/10.1016/B0-12-369397-7/00301-0>

92. Stracke, A.; Scherer, E.E.; Reynolds, B.C. Application of isotope dilution in geochemistry. *Treatise on Geochemistry*, 2nd ed., **2014**, 71–86. <https://doi.org/10.1016/b978-0-08-095975-7.01404-2>
93. Willbold, M.; Jochum, K.P. Multi-Element Isotope Dilution Sector Field ICP-MS: A Precise Technique for the Analysis of Geological Materials and its Application to Geological Reference Materials. *Geostand Geoanal Res*, **2005**, 29, 63–82. <https://doi.org/10.1111/j.1751-908x.2005.tb00656.x>
94. Raymond, P.A.; Saiers, J.E.; Sobczak, W.V. Hydrological and biogeochemical controls on watershed dissolved organic matter transport: pulse-shunt concept. *Ecology*, **2016**, 97, 5–16. <https://doi.org/10.1890/14-1684.1>
95. Siever, R.; Woodford, N. Dissolution kinetics and the weathering of mafic minerals. *Geochim Cosmochim Acta*, **1979**, 43, 717–724. [https://doi.org/10.1016/0016-7037\(79\)90255-2](https://doi.org/10.1016/0016-7037(79)90255-2)
96. Velbel, M.A. Influence of surface area, surface characteristics, and solution composition on feldspar weathering rates. In: *Geochemical Processes at Mineral Surfaces* J.A. Davis; K.F. Hayes; Eds. American Chemical Society Symposium Series No. 323, **1986**, 615–634
97. White, A.F.; Peterson, M.L. Chemical Modeling of Aqueous Systems II. *Acs Sym Ser*, **1990**, 461–475. <https://doi.org/10.1021/bk-1990-0416.ch035>
98. Appelo, C. A. J. Multicomponent Ion Exchange and Chromatography in Natural Systems. *Reviews in Mineralogy and Geochemistry 1* (34), 193–227.
99. Kahouli-Brahmi, S. Technological learning in energy–environment–economy modelling: A survey. *Energ Policy*, **2008**, 36, 138–162. <https://doi.org/10.1016/j.enpol.2007.09.001>
100. Nugent, M.A.; Brantley, S.L.; Pantano, C.G.; Maurice, P.A. The influence of natural mineral coatings on feldspar weathering. *Nature*, **1998**, 395, 588–591. <https://doi.org/10.1038/26951>
101. White, A.F.; Brantley, S.L. The effect of time on the weathering of silicate minerals: why do weathering rates differ in the laboratory and field? *Chem Geol*, **2003**, 202, 479–506. <https://doi.org/10.1016/j.chemgeo.2003.03.001>
102. Béarat, H.; McKelvy, M.J.; Chizmeshya, A.V.G.; Gormley, D.; Nunez, R.; Carpenter, R.W.; Squires, K.; Wolf, G.H. Carbon Sequestration via Aqueous Olivine Mineral Carbonation: Role of Passivating Layer Formation. *Environ Sci Technol*, **2006**, 40, 4802–4808. <https://doi.org/10.1021/es0523340>
103. Daval, D.; Calvaruso, C.; Guyot, F.; Turpault, M.-P. Time-dependent feldspar dissolution rates resulting from surface passivation: Experimental evidence and geochemical implications. *Earth Planet Sc Lett*, **2018**, 498, 226–236. <https://doi.org/10.1016/j.epsl.2018.06.035>
104. Zhu, C.; Lu, P. Alkali feldspar dissolution and secondary mineral precipitation in batch systems: 3. Saturation states of product minerals and reaction paths. *Geochim Cosmochim Acta*, **2009**, 73, 3171–3200. <https://doi.org/10.1016/j.gca.2009.03.015>
105. Emmanuel, S.; Ague, J.J. Impact of nano-size weathering products on the dissolution rates of primary minerals. *Chem Geol*, **2011**, 282, 11–18. <https://doi.org/10.1016/j.chemgeo.2011.01.002>
106. White, A.F.; Schulz, M.S.; Lawrence, C.R.; Vivit, D.V.; Stonestrom, D.A. Long-term flow-through column experiments and their relevance to natural granitoid

- weathering rates. *Geochim Cosmochim Acta*, **2017**, *202*, 190–214.
<https://doi.org/10.1016/j.gca.2016.11.042>
107. Brantley, S.L.; Shaughnessy, A.; Lebedeva, M.I.; Balashov, V.N. How temperature-dependent silicate weathering acts as Earth's geological thermostat. *Science*, **2023**, *379*, 382–389. <https://doi.org/10.1126/science.add2922>
108. Austin, R.; Gatiboni, L.; Havlin, J. Soil Sampling Strategies for Site-Specific Field Management. NC State Extensions, 2020, <https://content.ces.ncsu.edu/soil-sampling-strategies-for-site-specific-field-management> (accessed 2023-05-08).
109. Allen, W.J.; Sapsford, S.J.; Dickie, I.A. Soil sample pooling generates no consistent inference bias: a meta-analysis of 71 plant–soil feedback experiments. *New Phytol*, **2021**, *231*, 1308–1315. <https://doi.org/10.1111/nph.17455>
110. Carroll, D. Ion exchange in clays and other minerals. *GSA Bulletin*, **1959**, *70*, 749–779. [https://doi.org/10.1130/0016-7606\(1959\)70\[749:ieicao\]2.0.co;2](https://doi.org/10.1130/0016-7606(1959)70[749:ieicao]2.0.co;2)
111. Sumner, M.E.; Miller, W.P. Cation Exchange Capacity and Exchange Coefficients. In: *Methods of Soil Analysis Part 3: Chemical Methods*. Sparks, D.L.; ed. SSSA Book Series 5, Soil Science Society of America, **1996**, 1201-1230.
112. Sparks, D.L. *Environmental soil chemistry*, 2nd ed. Academic Press, 2003., ISBN 9780126564464, <https://doi.org/10.1016/B978-012656446-4/50006-2>.